Vol. 4, No. 1, 2026
DOI: 10.61975/gjset.v4i1.117

ORIGINAL ARTICLE

Sustainable Plant-Assisted Production of Silver Nanoparticle Hybrids for Antimicrobial Use: Insights from *Chromolaena odorata* and Patchouli Oil

Liska Nova Pebriani[1], Pati Kemala[2], Ghazi Mauer Idroes[3], Widya Fatriasari[2,5], Khairan Khairan[1,4], and Rinaldi Idroes[1,4,*]

[1]Department of Chemistry, Faculty of Mathematics and Natural Sciences, Universitas Syiah Kuala, Banda Aceh 23111, Indonesia; [2] Research Center for Biomass and Bioproducts, National Research and Innovation Agency (BRIN), Kawasan KST BJ Habibie, Serpong, Tangerang Selatan 15314 Indonesia; [3]Department of Occupational Health and Safety, Faculty of Health Sciences, Universitas Abulyatama, Aceh Besar 23372, Indonesia; [4]Department of Pharmacy, Faculty of Mathematics and Natural Sciences, Universitas Syiah Kuala, Banda Aceh 23111, Indonesia; [5]Research Collaboration Center for Biomass-Based Nano Technology Cosmetic (BRIN), in Collaboration with Mulawarman University and BRIN, Samarinda, East Kalimantan 75119, Indonesia

* Correspondence: rinaldi.idroes@usk.ac.id

Article History

Received
6 February 2026

Accepted
19 April 2026

Available Online
30 April 2026

Keywords

Green synthesis
Nanoparticle characterization
Geothermal-sourced plant
Response surface methodology
Microbial assay

Abstract

This study developed a green synthesis approach for silver nanoparticles (AgNPs) using ethanolic extracts of *Chromolaena odorata* leaves (LCo) collected from geothermal areas, followed by post-synthesis incorporation of patchouli oil (PO) to improve antimicrobial performance. The synthesis was optimized using Response Surface Methodology (RSM) based on $AgNO_3$ concentration and pH, with surface plasmon resonance (SPR) as the response indicator. Successful formation of AgNPs was confirmed by characteristic SPR absorption in the visible region. Structural and morphological analyses indicated the involvement of plant-derived functional groups in nanoparticle stabilization, with predominantly spherical particles and some aggregation observed. Antimicrobial testing against *Staphylococcus aureus*, *Escherichia coli*, and *Candida albicans* showed that the PO-AgNPs-LCo system exhibited a slightly higher inhibition zone compared to AgNPs-LCo alone, indicating a marginal enhancement in antimicrobial activity. These results suggest that geothermal-derived plant extracts can be effectively utilized for AgNPs synthesis, while post-synthesis incorporation of natural oils may provide additional functional modification. However, the observed enhancement remains limited, indicating the need for further optimization and mechanistic studies. Overall, this work highlights a simple and eco-friendly route for developing plant-based antimicrobial nanomaterials.

Introduction

In recent years, microbial therapies using antibiotics have encountered major challenges, mainly due to the increasing resistance of most pathogenic microorganisms to commonly used antimicrobial agents [1–3]. This resistance has become more widespread, reducing the effectiveness of available treatments [3,4]. Furthermore, the absence of breakthroughs in developing new antibiotic classes over the past three decades highlights a critical gap in antimicrobial research [5]. Due to their potent antimicrobial effects and ability to target a wide range of harmful microorganisms, silver nanoparticles (AgNPs) have gained attention as a promising alternative [6,7]. Nevertheless, traditional methods for synthesizing AgNPs often rely on hazardous chemicals and contribute to environmental contamination, raising sustainability concerns [8]. Consequently, the need for greener and more sustainable synthesis approaches has been increasing, particularly those that employ plant-derived extracts as bio-based reducing and stabilizing agents, given their biocompatibility and ecological advantages [9,10].

Chromolaena odorata, a fast-growing invasive plant species, offers a sustainable and cost-effective source of bioactive compounds suitable for nanoparticle synthesis. Furthermore, plants originating from geothermal environments are exposed to unique abiotic stress conditions such as high temperature, sulfur content, and acidic soil, which may influence secondary metabolite production and potentially enhance their reducing capability [11–14]. However, comparative insights into how geothermal origin affects the physicochemical and antimicrobial performance of *C. odorata*-derived AgNPs are still limited. By integrating green synthesis with advanced optimization techniques, reaction conditions can be fine-tuned to achieve more consistent nanoparticle formation within the nanoscale range [15]. Moreover, patchouli oil, an essential oil rich in patchouli alcohol and a locally important agricultural product in Aceh, has been reported to exhibit antimicrobial activity and potential synergistic effects when combined with metallic nanoparticles [16,17]. Nevertheless, its application in combination with geothermal-derived *C. odorata* AgNPs remains underexplored. To the best of our knowledge, no previous study has simultaneously integrated geothermal-derived *C. odorata* for AgNPs synthesis, Response Surface Methodology (RSM)-based optimization, and patchouli oil post-synthesis incorporation within a single framework. This highlights a clear research gap that the present study aims to address.

This research aims to investigate the synthesis of AgNPs using *C. odorata* sourced from a geothermal area, emphasizing optimization of reaction conditions, comprehensive characterization, and antimicrobial evaluation. This study employs Response Surface Methodology (RSM) to refine the synthesis process by evaluating the influence of $AgNO_3$ concentration and pH on surface plasmon resonance (SPR) behavior [18–21]. The optimization process concentrated on two primary parameters: silver nitrate ($AgNO_3$) concentration (A) and pH level (B), to determine their combined influence on the SPR wavelength, which was examined through UV-Vis analysis [15]. The optimized AgNPs-LCo were subsequently combined with patchouli oil via post-synthesis incorporation. It is hypothesized that geothermal-derived *C. odorata* may enhance AgNPs formation due to increased phytochemical activity, while patchouli oil incorporation may provide a modest improvement in antimicrobial performance through combined physical and bioactive interactions. The antimicrobial efficacy of the resulting materials was tested against *Escherichia coli*, *Staphylococcus aureus*, and *Candida albicans*. Comprehensive characterization was conducted using UV–Vis spectroscopy, particle size analysis (PSA), FTIR, SEM–EDX, and XRD. By comparing AgNPs-LCo and PO-AgNPs-LCo, this study seeks to provide a contextual understanding of how environmental origin and post-synthesis modification influence nanoparticle behavior, contributing to the development of more sustainable antimicrobial nanomaterials.

Materials and Methods

Materials

C. odorata leaves (Figure 1a) were collected from the geothermal area of Ie Jue, Aceh Besar, Indonesia (5.8440° N, 95.5472° E; 300 m above sea level) (Figure 1b). The plant material was harvested, washed thoroughly, and processed immediately after collection. All chemicals, including silver nitrate ($AgNO_3$), Dragendorff's, Mayer's, Wagner's, and Liebermann–Burchard reagents, ferric chloride ($FeCl_3$), gelatin, sulfuric acid, magnesium powder, Mueller Hinton agar (MHA), and Sabouraud dextrose agar (SDA), were purchased from Sigma-Aldrich (St. Louis, MO, USA) and used without further purification. Gentamicin, vancomycin, and fluconazole were obtained from local pharmacies as reference antimicrobial agents. *Escherichia coli* (ATCC 25922), *Staphylococcus aureus* (ATCC 25923), and *Candida albicans* (ATCC 10231) were used as test microorganisms.

(a) (b)

Figure 1. (a) leaves of *C. odorata*; (b) location of the sampling of *C. odorata* leaves.

Sample Preparation and Extraction

Fresh leaves of *C. odorata* were washed, cut into small pieces, and air-dried for 7 days followed by additional drying under ventilation for 4 days at room temperature until constant weight was achieved. The dried leaves were ground into fine powder. The extraction procedure was adapted from a previously reported method [22]. 8 g of powdered sample was extracted with 100 mL ethanol (70%) at 70°C for 120 min. The mixture was filtered through Whatman No. 1 filter paper, and the filtrate was stored at 4°C for further use in phytochemical analysis and nanoparticle synthesis.

Phytochemical Screening

Qualitative phytochemical screening of the ethanolic extract was performed to detect the presence of phenolics, flavonoids, alkaloids, saponins, steroids, terpenoids, and tannins using standard protocols [23]. Alkaloids were identified using Dragendorff's, Mayer's, and Wagner's reagents. Saponins were detected by persistent foam formation after vigorous shaking with distilled water. Steroids and terpenoids were analyzed using the Liebermann–Burchard test. Phenolics were detected using $FeCl_3$ solution, flavonoids using magnesium powder reduction, and tannins using gelatin and sulfuric acid tests.

Determination of Total Flavonoid Content (TFC) and Total Phenolic Content (TPC)

TFC and TPC were quantified using UV–Vis spectrophotometry (Shimadzu UV-2500, Japan). For TFC, 5 mg of dried extract was dissolved in methanol and reacted with aluminum chloride ($AlCl_3$) and potassium acetate solution. After incubation at 25°C for 10 min, absorbance was measured at 440 nm[24]. For TPC, 5 mg extract was reacted with Folin–Ciocalteu reagent followed by sodium carbonate (Na_2CO_3) addition. The mixture was incubated at 25°C for 120 min, and absorbance was measured at 765 nm[24]. All analyses were performed in triplicate.

Desain of Experiments (DoE)

The synthesis of AgNPs-LCo was optimized using RSM based on a Central Composite Design (CCD). $AgNO_3$ concentration and pH were selected as the independent variables, while reaction temperature and extract concentration were kept constant to minimize experimental complexity and to focus on the primary factors influencing nanoparticle formation[16]. Although these parameters were not varied in this research, their impact on nanoparticle formation is well acknowledged, and future studies should explore them further to improve optimization. The ranges of $AgNO_3$ (0.757–9.242 mM) and pH (2.34–13.6) were adopted from previous studies [15] to ensure stable nanoparticle formation and reliable SPR responses for statistical modeling. Experimental design and randomization of runs were generated using Minitab 18.0. The complete CCD matrix and corresponding SPR responses are presented in Table 1.

Table 1. CCD matrix.

Runs	Variable code for [$AgNO_3$] (ppm)	Variable code for pH	[$AgNO_3$] (mM)	pH	SPR
1	1.414	0	9.242	8	425
2	0	1.414	5	13.6	444
3	1	-1	8	4	476
4	0	0	5	8	497
5	-1	-1	2	4	400
6	0	0	5	8	497
7	0	0	5	8	497
8	-1	1	2	12	416
9	0	0	5	8	497
10	0	0	5	8	497
11	0	-1.414	5	2.34	402
12	1	1	8	12	434
13	-1.414	0	0.757	8	400

Green synthesis AgNPs-LCo

The bioreduction of *C. odorata* extract was utilized to synthesize AgNPs-LCo, adapting the procedure from [25] with slight modifications. Briefly, plant extract was mixed with 5 mM $AgNO_3$ solution (1:9 v/v ratio) and stirred at 60 rpm under dark conditions for 24 h at room temperature. The formation of AgNPs was indicated by a color change from greenish to brown[26–28]. The reaction mixture was centrifuged at 10,000 rpm for 30 min, and the resulting pellet was collected and washed with distilled water. UV–Vis spectra were recorded in the range of 300–600 nm using quartz cuvettes (1 cm path length) to confirm SPR formation.

Green Hybrid synthesis AgNPs-LCo via patchouli

The preparation of hybrid AgNPs-LCo followed the method described by [16] with slight modifications. In this study, the term “hybrid” refers to a combined AgNPs–patchouli oil system formed via post-synthesis incorporation, rather than a chemically engineered nanostructure. The optimized conditions of the AgNPs-LCo synthesis process involved mixing with patchouli oil to form hybrid nanoparticles. The PO used in this study was a heavy fraction of PO refined from crude oil [17]. The process of refining PO has been described in previous studies. The hybridization process of AgNPs-LCo with patchouli oil (PO) was initiated by synthesizing AgNPs-LCo under the optimized reaction conditions identified through the RSM approach. After an initial 12-hour incubation, 4 mL of PO was gradually introduced into the system. The mixture was subsequently incubated for an additional 24 hours under stirring 60 rpm at room temperature to ensure complete interaction between the components. The final hybrid material obtained from this process was referred to as PO-AgNPs-LCo.

Characterization of AgNPs-LCo and PO-AgNPs-LCo

The characterization of AgNPs-LCo and PO-AgNPs-LCo was conducted using a series of advanced analytical techniques to comprehensively evaluate their structural, morphological, and elemental properties. UV–Vis spectroscopy (Shimadzu UV-2500) was used to confirm SPR peaks (300–600 nm). FTIR analysis (Agilent Cary 630) was performed in the range of 4000–400 cm^{-1} to identify functional groups. Particle size distribution was analyzed using Dynamic Light Scattering (DLS) (Shimadzu SALD-2300). Crystallinity was determined using X-ray diffraction (XRD, Empyrean Series 3, PANalytical, Netherlands) with Cu Kα radiation (λ = 0.15406 nm) over 2θ = 10–80°. Surface morphology and elemental composition were analyzed using SEM-EDS (Carl Zeiss EVO MA 10) at 20 kV accelerating voltage.

Antimicrobial activity test

Antimicrobial activity was evaluated using the Kirby–Bauer disk diffusion method according to Clinical and Laboratory Standards Institute (CLSI M02) guidelines. Bacterial inoculum was adjusted to 0.5 McFarland standard and uniformly spread onto Mueller–Hinton Agar (MHA) plates using a sterile swab. For antifungal testing, Sabouraud Dextrose Agar (SDA) was used

and inoculated with Candida albicans under the same standardization procedure. Sterile paper discs (6 mm diameter) were placed on the agar surface and loaded with 50 µL of sample solution, including AgNPs-LCo and PO-AgNPs-LCo. Plates were allowed to dry under sterile conditions before incubation. Bacterial plates were incubated at 37°C for 24 h, while fungal plates were incubated at 28–30°C for 48 h. After incubation, inhibition zones were measured in millimeters. Vancomycin (30 µg), gentamicin (10 µg), and fluconazole (25 µg) were used as positive controls for *S. aureus*, *E. coli*, and *C. albicans*, respectively. Ethanol was used as negative control. All experiments were performed in triplicate.

Results and Discussion

Phytochemical Screening

The *C. odorata* samples used in this study were collected from plants thriving in the geothermal area of Ie Jue, situated in Aceh, Indonesia. This region is notable for its naturally occurring thermal springs enriched with sulfur, exhibiting mildly acidic conditions (pH 5.77 ± 0.04). The area is also enveloped by hot vapors with a high sulfur content [29]. Surface water measurements indicated a temperature of 93.55 ± 0.64°C, with notable conductivity and high total dissolved solids (TDS) concentrations. The turbidity of the hot spring water was attributed to acidic clay content. Phytochemical analysis confirmed the presence of various bioactive compounds in the plant extract, including phenolics, alkaloids, flavonoids, saponins, steroids, and tannins. However, no terpenoid content was identified, as detailed in Table 2.

Table 2. Contents of phytochemicals in the *C. odorata* ethanolic leaf extract

Secondary metabolites	Result
Phenolics	+
Flavonoids	+
Alkaloids	+
Saponin	+
Steroids	+
Terpenoids	-
Tannins	+

Description: (+) detected, (-) not detected

Plants that thrive in extreme conditions often produce unique secondary metabolites or accumulate them in substantial amounts as a survival mechanism[11,30]. This characteristic influenced the selection of *C. odorata* for this research. Bioactive secondary metabolites are crucial in the green synthesis of AgNPs, prompting a phytochemical analysis of *C. odorata* leaf extract to determine its chemical profile[9]. As shown in Table 2, the analysis confirmed the presence of phenolics, flavonoids, alkaloids, saponins, steroids, and tannins, whereas terpenoids were absent. Prior research has identified *C. odorata* as a rich source of bioactive compounds, including flavonoids, fatty acids, saponins, and alkaloids, with flavonoids and alkaloids being the primary contributors to its antimicrobial properties[31].

The ethanolic extract of *C. odorata* showed the presence of phenolic and flavonoid compounds, with concentrations determined as 11.84 ± 0.001 mg GAE/g and 5.43 ± 0.0006 mg QE/g, respectively. Method validation was performed using the LINEST function in Microsoft Excel, and the evaluated parameters are presented in Table 3, including limits of detection (LoD), limits of quantification (LoQ), coefficient of determination (R^2), relative standard deviation (%RSD), percentage recovery (%R), and measurement uncertainty.

Table 3. Validation of the method.

Parameter	LoD	LoQ	R^2	%RSD	%R
TFC	33.86	102.60	0.9789	2.34	97.55
TPC	54.96	166.54	0.9479	1.00	122.28

However, differences in analytical performance were observed between the two assays. The TPC method showed relatively lower linearity (R^2 = 0.9479) and an out-of-range recovery value (%R = 122.28%), which may indicate matrix effects or experimental variability during the assay. Therefore, the TPC results should be interpreted as indicative rather than fully validated quantitative values. In contrast, the TFC method showed better analytical performance, with acceptable linearity (R^2 = 0.9789) and low %RSD (2.34%), suggesting that it is relatively more reliable for comparative evaluation of flavonoid content in this study.

Design of experiment (DoE) based optimization

In this study, the DoE applied a CCD to evaluate the influence of various factors, specifically $AgNO_3$ concentration and pH, on the response variable, which corresponds to the experimental SPR determined through UV-Vis analysis. Table 4 presents the ANOVA results obtained from the experiment.

Table 4. ANOVA findings from the experiment.

Source	DF	Adj SS	Adj MS	F -Value	P -Value
Model	5	24061.2	4812.2	19.59	0.001
Linear	2	2231.0	1115.5	4.54	0.054
[$AgNO_3$]	1	2091.6	2091.6	8.51	0.022
pH	1	139.4	139.4	0.57	0.476
Square	2	20989.1	10494.6	42.72	0.000
[$AgNO_3$]*[$AgNO_3$]	1	13353.3	13353.3	54.36	0.000
pH*pH	1	10344.8	10344.8	42.11	0.000
2-Way Interaction	1	841.0	841.0	3.42	0.107
[$AgNO_3$]*pH	1	841.0	841.0	3.42	0.107
Error	7	1719.6	245.7		
Lack-of-Fit	3	1719.6	573.2	Undefined	Undefined
Pure Error	4	0.0	0.0		
Total	12	25780.8			

The developed regression model was found to be statistically significant (p = 0.001), indicating that the selected variables contributed to the observed response. The reliability and statistical significance of the regression-based mathematical model were evaluated by considering the p-value and Fisher's test statistic. Among the linear terms, $AgNO_3$ concentration showed a statistically significant effect ($p < 0.05$), whereas pH did not exhibit a significant linear influence. However, the quadratic terms were highly significant ($p < 0.001$), suggesting the presence of non-linear effects in the system. In contrast, the interaction between $AgNO_3$ concentration and pH was not statistically significant ($p > 0.05$), indicating a limited combined effect of these variables under the studied conditions. To explore the relationship among the concentration of the silver precursor, pH level and the SPR wavelength as the response parameter, additional statistical analysis was conducted. This interaction was then visually depicted through three-dimensional surface plots and contour plots, which are presented in Figure 2a and Figure 2b.

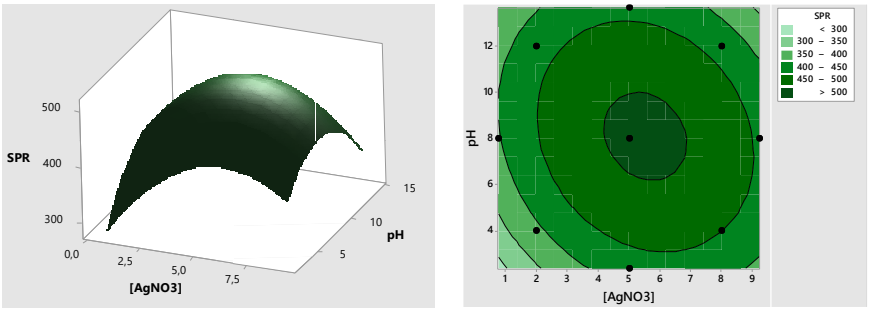

Figure 2. (a) 3D response surface and (b) 2D contour map depicting the relationship between [$AgNO_3$], pH and the SPR properties of AgNPs-LCo.

The regression equation describing the SPR response is given in Equation (1), which was used to predict and validate the optimal synthesis conditions.

$$SPR = 361{,}07 + 7{,}816\ [AgNO_3] + 9.060\ pH - 0.5486\ [AgNO_3][AgNO_3] \\ -0.4336\ pH \times pH - 0.3542\ [AgNO_3] \times pH \quad (1)$$

This equation was used to describe and predict the SPR behavior within the studied experimental domain. A limitation of the model is the absence of pure error in the experimental design, which prevented a valid lack-of-fit evaluation. Therefore, although the model is statistically significant, its predictive capability should be interpreted cautiously, particularly outside the tested range. From a mechanistic perspective, variations in SPR are associated with changes in nanoparticle size and distribution, where shifts toward shorter wavelengths are generally related to smaller particle sizes. This trend has been widely reported in silver nanoparticle systems [32] Based on the RSM analysis, the optimal synthesis condition was identified at 5 mM $AgNO_3$ and pH 8, which produced a stable and consistent SPR response within the experimental dataset, indicating controlled nanoparticle formation under the optimized conditions.

Synthesis of AgNPs-LCo and Hybrid (PO-AgNPs–LCo) System

Based on the RSM optimization results, the synthesis of AgNPs-LCo was subsequently carried out under the identified optimal conditions (5 mM $AgNO_3$ and pH 8). The successful formation of AgNPs-LCo was initially indicated by a visible color change in the reaction mixture. The ethanolic extract of *C. odorata* exhibited a green color, while the solution gradually turned dark brown after interaction with $AgNO_3$ (Figure 3a–c), confirming the reduction of Ag^+ to Ag^0. This color transition is attributed to SPR of AgNPs and is commonly reported in plant-mediated nanoparticle synthesis systems [33–38]. The observed change confirms that phytochemical constituents in *C. odorata*, particularly phenolic and flavonoid compounds identified in the extract, act as reducing as well as stabilizing agents during nanoparticle formation. These bioactive molecules facilitate electron transfer processes that drive the reduction of silver ions and subsequent nucleation of nanoparticles.

(a) (b) (c) (d)

Figure 3. Representative images showing (a) the ethanolic extract derived from *Chromolaena odorata* leaves, (b) freshly prepared AgNPs-LCo solution prior to incubation, (c) AgNPs-LCo solution following the incubation process, and (d) PO-AgNPs-LCo sample.

After nanoparticle formation, patchouli oil (PO) was introduced into the system. The resulting dispersion exhibited a brown and slightly heterogeneous appearance (Figure 3d), suggesting limited miscibility between the aqueous nanoparticle colloid and the hydrophobic oil phase. In this study, the term “hybrid” refers to a combined system rather than a chemically defined nanostructure. Based on the experimental observations and methodological limitations, the interaction between AgNPs and PO is considered predominantly physical in nature, most likely

involving surface adsorption of oil constituents onto AgNPs surfaces and partial dispersion within the colloidal system, rather than chemical bonding or structured encapsulation. Therefore, no specific hybrid architecture can be confirmed from the present data. The use of refined PO (heavy fraction, ~60.66% patchouli alcohol) is relevant due to its reported antimicrobial properties [39]. However, in the present system, its role is interpreted as a surface-interacting organic phase that may influence colloidal behavior rather than forming a chemically integrated hybrid structure.

Characterization

UV–Visible spectrophotometric analysis confirmed the formation of AgNPs-LCo through the appearance of surface plasmon resonance (SPR) bands in the 300–600 nm range, with maxima at 497 nm (AgNPs-LCo) and 473 nm (PO-AgNPs-LCo) (Figure 4a). The observed blue shift after PO incorporation suggests changes in the local dielectric environment and possible surface modification of nanoparticles rather than new nanoparticle formation. This SPR phenomenon is consistent with the unique optical properties of metallic nanoparticles, where light absorption and scattering occur at specific wavelengths due to collective electron oscillation [40]. The shift in SPR position has also been widely associated with changes in particle size and surrounding medium in green-synthesized AgNPs systems [40]. Studies on AgNPs synthesized via green synthesis using *Cymbopogon citratus*, *Amorphophallus paeoniifolius*, *Trichoderma reesei*, *Lantana camara*, and *Calotropis gigantea* reported SPR peaks at 470, 446, 438, 417, and 450 nm[15,27,33,41,42].

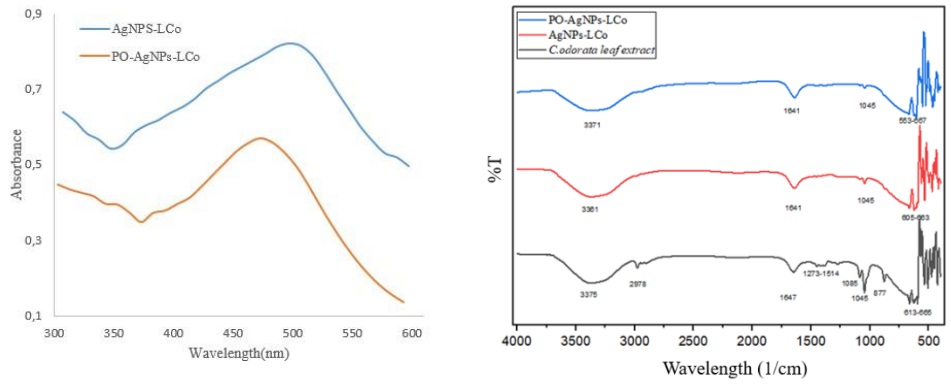

(a) (b)

Figure 4. (a) UV Vis and (b) FTIR spectra.

Figure 4b presents the FTIR spectral analysis of the plant extract, AgNPs-LCo, and PO-AgNPs-LCo, displaying characteristic absorption peaks at 3371, 1641, 1045, 877, and 600 cm^{-1}. The observed signals correspond to —OH, N—H, C—N, and C—H functional groups, which play a crucial role in facilitating the green synthesis process. This finding aligns with earlier studies that also confirmed the presence of —OH[28,43–46], —NH [37,44,47], C—N [37,47], and C–H [35] during the green synthesis of AgNPs.

Particle size analysis revealed that AgNPs-LCo exhibited an average size of 93 ± 0.188 nm (Figure 5), confirming successful nanoscale formation. This size is comparable to previously reported plant-mediated AgNPs, including those synthesized under geothermal conditions, indicating that environmental and phytochemical variability significantly influences nanoparticle size[38]. Variations in particle size among green synthesis systems have been widely reported and are attributed to differences in extract composition, which acts as both reducing and stabilizing agents [48]. This supports the role of bioactive compounds in controlling nucleation and growth processes. Moreover, the findings confirm that RSM serves as a reliable method for predicting and fine-tuning reaction conditions in green synthesis.

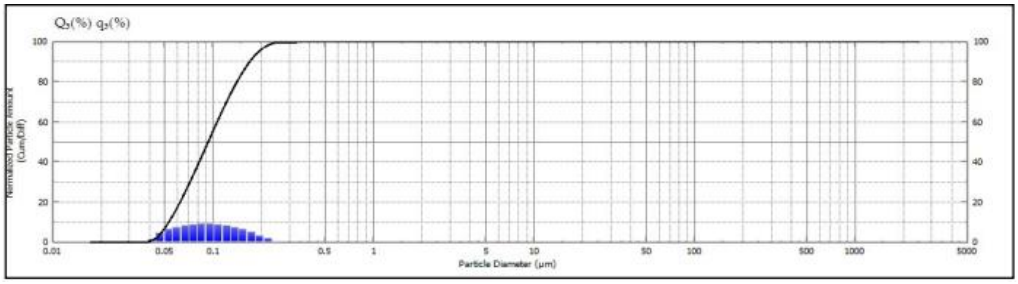

Figure 5. Measurement of AgNP-LCo particle size distribution utilizing a PSA.

The SEM analysis reveals that most of the observed structures morphologies of the AgNPs-LCo are spherical, whereas a portion exhibit irregular shapes and agglomeration (Figure 6a). Conversely, PO-AgNPs-LCo exhibits an irregular and agglomerated morphology (Figure 6b).

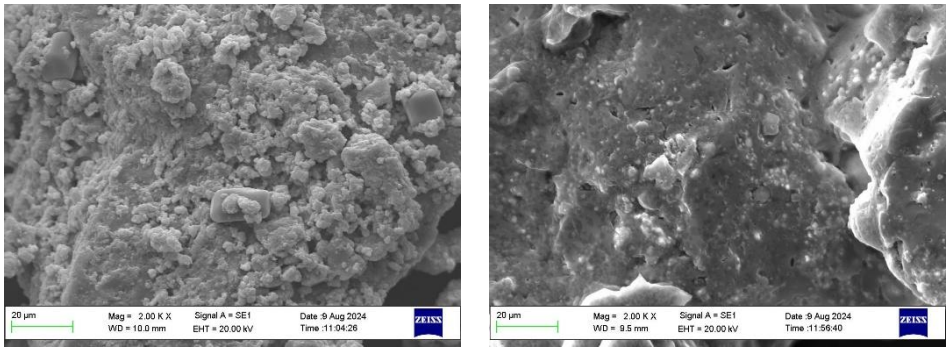

(a) (b)

Figure 6. SEM image of (a) AgNPs-LCo and (b) PO-AgNPs-LCo displayed at 20,000× magnification.

Additionally, SEM examination was performed to evaluate the dimensions and morphological characteristics of the synthesized nanoparticles. As shown in Figure 6, both AgNPs-LCo and PO-AgNPs-LCo exhibited irregular shapes with uniform size and noticeable agglomeration. While the nanoparticles were predominantly spherical, some displayed polygonal shapes. Interestingly, the agglomeration of silver nanoparticles can impact their antimicrobial activity. A study published in *Scientific Reports* discusses the characteristics and antibacterial properties of AgNPs synthesized using plant extracts, emphasizing that particle size and distribution influence their antibacterial effectiveness [49]. Although the study does not explicitly state that agglomeration enhances activity, its findings highlight the importance of controlling nanoparticle size and morphology to optimize their antimicrobial performance [50]. Additionally, other plant-based AgNPs synthesized from *Calotropis gigantea* [44] and *Lantana Camara* [15] collected from geothermal sites have demonstrated similar morphological characteristics to those observed in this study.

EDS spectroscopy was utilized to examine the elemental makeup of the samples [27]. The resulting EDS spectra for AgNPs-LCo and PO-AgNPs-LCo are presented in Figure 7. Silver atoms make up 49.26% of the AgNPs-LCo sample, with sodium (1.64%), carbon (14.33%), chlorine (8.58%), and oxygen (14.83%) following closely behind. In contrast, PO-AgNPs-LCo contained silver (25.93%), oxygen (18.98%), carbon (44.33%), nitrogen (5.13%), sodium (0.69%), aluminium (0.15%), and chlorine (1.91%).

The AgNPs-LCo sample is composed of 49.26% silver atoms, with sodium (1.64%), carbon (14.33%), chlorine (8.58%), and oxygen (14.83%) present in close succession. On the other hand, PO-AgNPs-LCo showed nitrogen (5.13%), sodium (0.69%), aluminum (0.15%), chlorine (1.91%), silver (25.93%), oxygen (18.98%), and carbon (44.33%). The detection of carbon, chlorine, and oxygen suggests the possible existence of residual organic substances on the surface of the nanoparticles[51]. Additionally, the identification of nitrogen and aluminum after

the hybridization of AgNPs with PO has been documented in previous research [17]. Furthermore, a study by [56,63] reported that in plant-based synthesis of AgNPs, EDX analysis commonly detects not only silver but also minor signals of elements such as oxygen, carbon, chlorine, and aluminum, which are attributed to biomolecules adsorbed onto the nanoparticle surface during synthesis. This suggests that the presence of chlorine and aluminum in our sample may similarly originate from phytochemicals or residual components in the plant extract and PO matrix used during synthesis. This explanation strengthens the hypothesis that the elemental composition, particularly on the nanoparticle surface, may influence its functional properties, including antimicrobial activity.

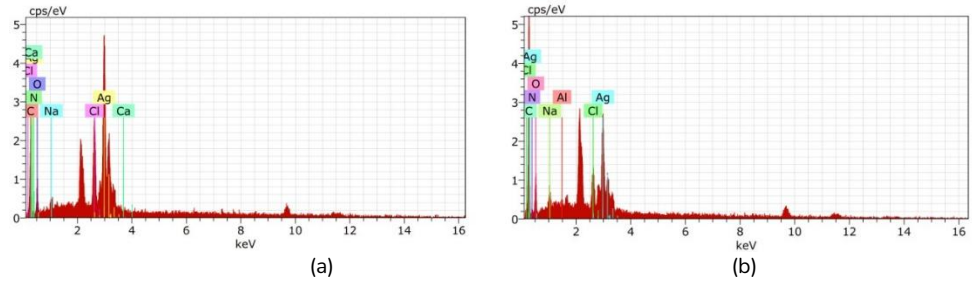

Figure 7. EDX results of (a) AgNPs-LCo and (b) PO-AgNPs-LCo

The XRD pattern analysis verified the successful formation of silver nanoparticles derived from *C. odorata* leaves, confirming their crystalline characteristics. As illustrated in Figure 8, the XRD diffractogram exhibits distinct Miller indices at (111), (200), (220), (222), and (311). The Scherrer equation was utilized to determine the crystallite size of the synthesized AgNPs, linking the broadening of XRD peaks to nanoparticle dimensions.

Moreover, the XRD analysis (Figure 8) verified that the synthesized nanoparticles possess a crystalline structure, as demonstrated by distinct diffraction patterns linked to Miller indices (111), (200), (220), (222), and (311). These diffraction signals confirm the development of a face-centered cubic (FCC) crystal lattice, which is a well-known characteristic of silver nanoparticles. This ordered and symmetric FCC structure predicts favorable physical and chemical qualities, such as strong mechanical strength and thermal stability. Using the Scherrer equation, the calculated crystal sizes of AgNPs-LCo and PO-AgNPs-LCo were 29.05 nm and 37.96 nm, respectively. XRD-based crystal size analysis for AgNPs-LCo (29.05 nm) contrasts with the 93 nm particle size obtained via PSA. [53] and [54] explained that these discrepancies arise from measurement techniques: PSA assesses hydrodynamic sizes, which are typically larger due to agglomeration effects, via dynamic light scattering (DLS), whereas XRD measures the crystalline domains within the nanoparticles. The latter provides crystal domain sizes, often smaller than the total particle size detected by PSA, as it does not account for agglomeration [55].

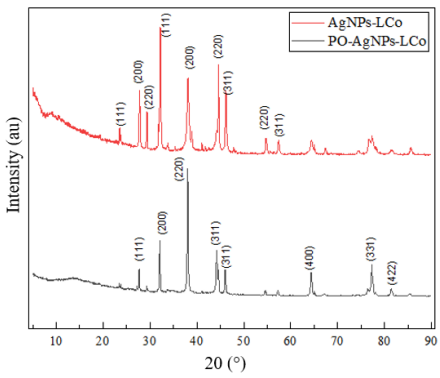

Figure 8. XRD of AgNPs-LCo and PO-AgNPs-LCo.

In the Equation (2), *D* denotes the size of the crystallite (measured in nanometers), while *K* refers to the shape factor, which is generally assigned a value of 0.9 for spherical nanoparticles. The parameter λ represents the X-ray wavelength, commonly 0.15406 nm for Cu Kα radiation, while β denotes the full width at half maximum (FWHM) of the diffraction peak in radians, and θ corresponds to the Bragg diffraction angle in degrees. The FWHM values were derived from the XRD patterns using Gaussian peak fitting, and the crystallite size was determined based on the most intense diffraction peak. This method offers insight into the average crystallite dimensions within the synthesized sample [56].

$$D = K\,\lambda\,/\,\beta\,cos\,cos\,\theta \qquad (2)$$

Antimicrobial activity

The inhibition zone measurements are presented as mean values along with their corresponding standard deviations (SD). Based on the data in Table 5, the addition of PO in the synthesis of PO-AgNPs-LCo resulted in a slight improvement in antimicrobial activity compared to AgNPs-LCo alone. Specifically, the inhibition zones increased by 0.98 mm for *S. aureus*, 0.70 mm for *E. coli*, and 0.98 mm for *C. albicans*. The findings of antibacterial and antifungal activity are presented in Table 5 and Figure 9. Interestingly, silver nitrate solution did not exhibit antibacterial effects under the tested conditions. However, incorporation of PO with AgNPs-LCo led to a slight enhancement in antimicrobial response. It should be noted that the ethanolic extract of *C. odorata* was not evaluated independently in this study. Therefore, the individual contribution of plant-derived bioactive compounds cannot be clearly distinguished. In addition, a patchouli oil-only control was not included, which limits the interpretation of whether the observed effect is additive or potentially interactive in nature. Thus, the antimicrobial response should be considered preliminary. Therefore, the material is more appropriately described as a potential adjunct antimicrobial agent rather than a standalone therapeutic substitute for conventional antibiotics, and further studies including appropriate control systems and combination assays are required.

Table 5. Antimicrobial activity.

	Inhibition Zone, Mean Value ± Standard Deviation (mm)		
Sample	***Staphylococcus aureus***	***Escherichia coli***	***Candida albicans***
AgNPs-LCo	10.45±0.22	9.49±0.11	7.29±0.28
PO-AgNPs-LCo	11.43±0.33	10.19±0.12	8.27±0.07
Ethanol	0.00±0.00	0.00±0.00	0.00±0.00
Control	16.58±0.13[a]	24.38±0.11[b]	25.17±0.13[c]

Control (+): [a]vancomycin, [b]gentamicin, and [c]fluconazole

Comparisons between the geothermal and non-geothermal conditions for *C. odorata*-based AgNPs synthesis, as well as the effects of hybridizing AgNPs with PO are presented in Table 6. The synthesis of AgNPs using *C. odorata* from geothermal and non-geothermal areas revealed differences in their properties (Table 6). Compared with their non-geothermal counterparts, the AgNPs-LCo synthesized under geothermal conditions showed a higher SPR peak (497 nm) and larger average particle size (93 nm), whereas the non-geothermal counterpart exhibited an SPR peak at 429 nm and a smaller particle size (15.27 nm). Low SPR values are generally associated with smaller particle sizes [32]. These differences indicate variation in nanoparticle formation behavior under different environmental growth conditions of the plant source. Morphologically, geothermal-plant-sourced AgNPs were spherical with some irregular shapes and aggregation, while non-geothermal-plant-sourced AgNPs were more uniformly spherical. The geothermal AgNPs exhibited stronger antimicrobial effects against *S. aureus* compared to their lower effectiveness against E. coli and C. albicans. In contrast, non-geothermal AgNPs showed moderate antibacterial and excellent antifungal activity, indicating potential pathogen specificity based on the synthesis environment.

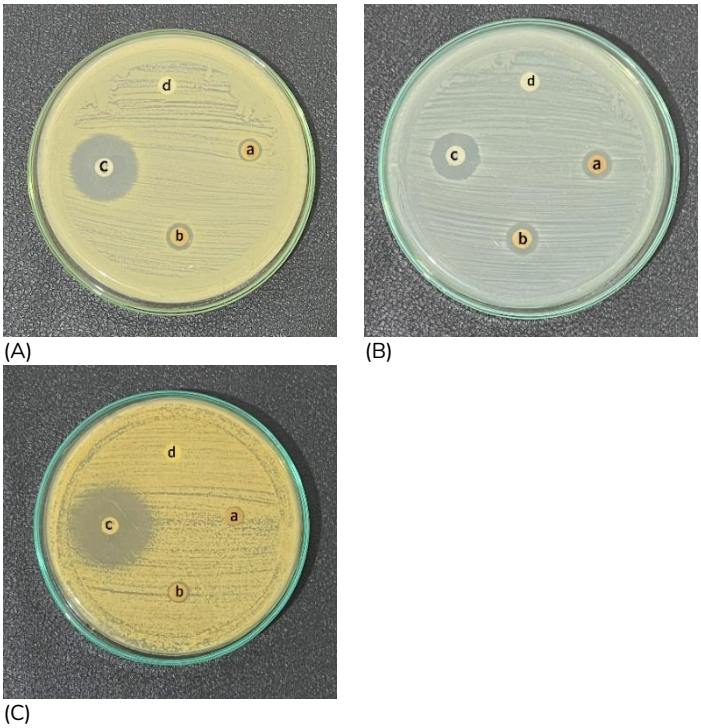

Figure 9. Evaluation of the antimicrobial properties of AgNPs-LCo against (A) *E. coli* bacteria, (B) *S. aureus* bacteria, and (C) *C. albicans* fungus. In this analysis, (a) corresponds to AgNPs-LCo, (b) represents PO-AgNPs-LCo, (c) denotes the positive control, and (d) refers to ethanol.

Table 6. Comparative analysis of AgNPs synthesis in geothermal and non-geothermal environments.

Parameters	AgNPs-LCo		AgNPs hybridized with other POs		
	Geothermal Conditions	**Non-Geothermal Conditions** [57]	**PO-AgNPs-LCo (This Study**	**HP-AgNPs-LCg** [17]	**P-Ag-NPs-HBE** [16]
Source of plant material	*C. odorata* growing in geothermal area	*C. odorata* growing in non-geothermal area	*C. odorata* from geothermal area + PO	*Calotropis gigantea* from geothermal area + PO	*Lablab purpureus* + PO
Reaction optimization using RSM	pH 8.5 mM $AgNO_3$, 25°C	-	pH 8.5 mM $AgNO_3$, 25°C	pH 9.4 mM $AgNO_3$, 25°C	pH 4.126, 1.031 mM $AgNO_3$, 25°C
SPR	497 nm	429 nm	473 nm	360 nm	415 nm
Particle size (Average)	29.05 nm	15.27 nm	n.d	422 nm	110 nm
Shape	Spherical, with some irregular and agglomerated forms	Spherical shapes	irregular and agglomerated shapes	Cubic with some spherical forms, with an oil layer.	Spherical with a thin PO outer layer
Microbial inhibition potential	More potent against *S. aureus* than *E. coli* and *C. albicans*.	Shows moderate inhibition against bacteria yet excels in antifungal activity.	PO enhanced the antimicrobial activity of AgNPs-LCo, with stronger effects on *S. aureus* and *C. albicans* than on *E. coli*.	PO enhanced AgNPs-LCg antimicrobial activity, highest against *S. aureus*, followed by *E. coli*, and lowest against *C. albicans*.	PO improved the antibacterial efficacy of AgNPs against *E. coli*, as this study did not assess other pathogenic microbes.

AgNPs hybridized with PO showed variable properties and efficacy depending on the plant source. The PO-AgNPs-LCo synthesized using geothermal *C. odorata* showed increased antimicrobial potency against *S. aureus* and *C. albicans*. This improvement highlights the synergistic interaction between AgNPs and the bioactive compounds present in PO, which collectively enhance antimicrobial efficacy. However, the nanoparticles had irregular shapes with clumping. AgNPs hybridized with oils from other plants, such as *Calotropis gigantea* (HP-AgNPs-LCg) and *Lablab purpureus* (P-AgNPs-HBE), presented distinct characteristics. The HP-AgNPs-LCg primarily exhibited a cubic morphology, with some spherical structures also observed. It displayed a lower SPR peak at 360 nm and a notably larger particle size of 422 nm, which could potentially limit its bioavailability. P-AgNPs-HBE, with an SPR peak at 415 nm and spherical morphology, had a moderate particle size (110 nm) and was effective against *E. coli*. These findings highlight the variability introduced by different plant sources and the potential of PO hybridization to increase AgNPs performance, albeit with challenges such as size inconsistency and agglomeration. A limitation of this study is the lack of investigation into the chemical and biological stability of the synthesized AgNPs-patchouli oil hybrids over time. The stability conditions of the hybrids under various storage or environmental conditions were not evaluated, which may affect their long-term applicability.

In general, AgNPs may contribute to microbial inhibition through membrane interaction, intracellular penetration, and induction of oxidative stress [44,58]. Additionally, interactions between AgNPs and bacterial membranes have been reported to affect membrane permeability [59], thereby potentially inhibiting bacterial replication. In this study, a dual-action hypothetical mechanism is proposed based on previously reported literature. It is suggested that AgNPs may contribute to cellular damage and reactive oxygen species (ROS) generation, while phytochemical components from patchouli oil may disrupt membrane integrity and interact with bacterial proteins, resulting in multi-target stress on microbial cells [60], Patchouli oil components have also been reported to potentially increase membrane fluidity, which may facilitate the entry of AgNPs and Ag^{+} ions into bacterial cells (Figure 10). However, it should be emphasized that this mechanism has not been experimentally validated in the present study, and a complete understanding of the synergistic antibacterial mechanism is still under investigation [61].

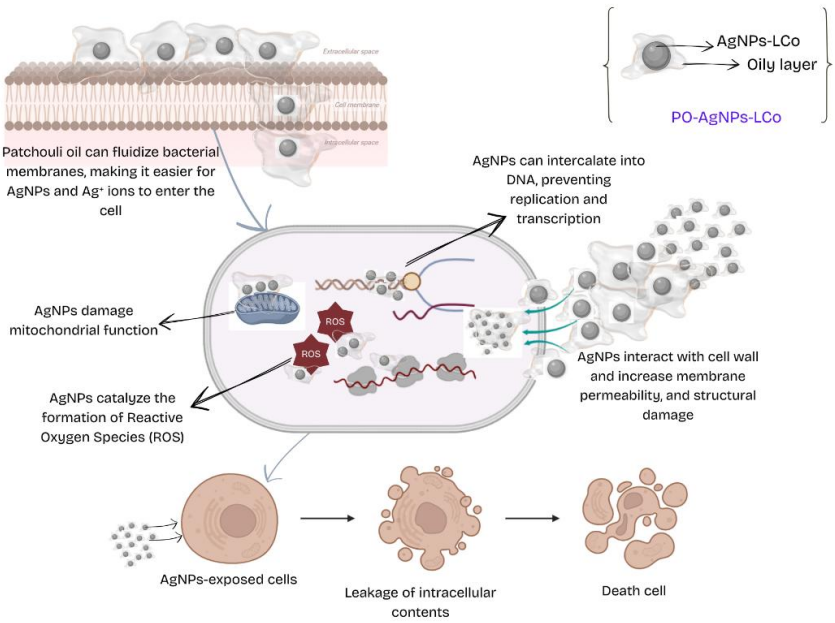

Figure 10. Proposed antibacterial interaction mechanism of silver nanoparticles and patchouli oil against bacterial cells.

This study underscores the role of environmental factors, particularly geothermal conditions, in influencing the phytochemical profile of plant materials and, consequently, the properties of biosynthesized AgNPs. The post-synthesis incorporation of PO provides a simple yet effective strategy to modify nanoparticle behavior and potentially modulate antimicrobial performance, although issues such as particle agglomeration and size heterogeneity remain challenges that require further optimization. The findings highlight that both synthesis conditions and post-synthesis modification play important roles in determining the structural and functional characteristics of AgNPs systems. In addition, this work demonstrates a combined green synthesis–post modification approach that contributes to the development of tunable AgNPs-based materials. Future studies should focus on optimizing reaction parameters, elucidating interaction mechanisms between AgNPs and organic phases, and expanding antimicrobial assessments to a broader range of pathogens. Further investigation into stability and long-term behavior is also essential to support potential biomedical applications such as wound healing, topical antimicrobial systems, and drug delivery platforms.

Conclusions

This study demonstrated the green synthesis of AgNPs using *C. odorata* leaf extract derived from geothermal areas, followed by post-synthesis incorporation of patchouli oil (PO) to form a combined AgNPs–organic system. The synthesis under optimized RSM conditions (5 mM $AgNO_3$ and pH 8) produced AgNPs-LCo with an SPR peak at 497 nm and an average particle size of 93 nm, which was larger than the non-geothermal counterpart reported in previous studies (15.27 nm), indicating that geothermal-derived plant material influences nanoparticle properties rather than necessarily reducing particle size. The incorporation of PO resulted in a slight increase in antimicrobial activity against *Staphylococcus aureus*, *Escherichia coli*, and *Candida albicans*, with inhibition zone improvements ranging from 0.70–0.98 mm. However, this enhancement should be considered marginal, as no statistical significance or formal synergy assessment (e.g., FIC index) was performed. Therefore, the observed effect is better interpreted as an additive or complementary contribution rather than confirmed synergy.

A key limitation of this study is the absence of stability evaluation of the PO-AgNPs–LCo system as well as the lack of individual control testing for plant extract and patchouli oil contributions, which restricts deeper mechanistic interpretation. In addition, antimicrobial evaluation was limited to inhibition zone assays without MIC or MBC determination. Despite these limitations, the study highlights the potential of integrating geothermal-sourced plant extracts with post-synthesis organic modification as a tunable and environmentally friendly approach for AgNPs fabrication. Future work should focus on stability analysis, quantitative antimicrobial assays (MIC/MBC), cytotoxicity evaluation, and mechanistic synergy validation to better assess the biomedical applicability of this system.

Funding: This study does not receive external funding.

Ethical Clearance: Not applicable.

Informed Consent Statement: Not applicable.

Data Availability Statement: The data that support the findings of this study are available from the corresponding author upon reasonable request.

Conflicts of Interest: All the authors declare no conflicts of interest.

References

[1] Maulana I, Fasya D, Ginting B. Biosynthesis of Cu Nanoparticles Using Polyalthia Longifolia Roots Extracts for Antibacterial, Antioxidant and Cytotoxicity Applications. *Materials Technology* 2022;37:2517–21. https://doi.org/10.1080/10667857.2022.2044217.

[2] Althubiti AA, Alsudir SA, Alfahad AJ, Alshehri AA, Bakr AA, Alamer AA, et al. Green Synthesis of Silver Nanoparticles Using Jacobaea Maritima and the Evaluation of Their Antibacterial and Anticancer Activities. *International Journal of Molecular Sciences* 2023;24. https://doi.org/10.3390/ijms242216512.

[3] Singh H, Du J, Yi TH. Biosynthesis of Silver Nanoparticles Using Aeromonas Sp. THG-FG1.2 and Its Antibacterial Activity against Pathogenic Microbes. *Artificial Cells, Nanomedicine and Biotechnology* 2017;45:584–90. https://doi.org/10.3109/21691401.2016.1163715.

[4] Rumangu CP, Fatimawali F, Manampiring AE, Kepel BJ, Budiarso FDH, Bodhi W. Evaluating the Efficacy of Clerodendrum Minahassae Ethanol Extract on Insulin Regulation in Diabetic Wistar Rats. *Malacca Pharmaceutics* 2024;2:18–23. https://doi.org/10.60084/mp.v2i1.137.

[5] Szewczuk MA, Zych S, Oster N, Karakulska J. Activity of Patchouli and Tea Tree Essential Oils against Staphylococci Isolated from Pyoderma in Dogs and Their Synergistic Potential with Gentamicin and Enrofloxacin. *Animals* 2023;13. https://doi.org/https://doi.org/10.3390/ani13081279.

[6] Crisan CM, Mocan T, Manolea M, Lasca LI, Tăbăran FA, Mocan L. Review on Silver Nanoparticles as a Novel Class of Antibacterial Solutions. *Applied Sciences (Switzerland)* 2021;11:1–18. https://doi.org/10.3390/app11031120.

[7] Fakri F, Harahap SP, Muhni A, Khairan K, Hewindati YT, Idroes GM. Antimicrobial Properties of Medicinal Plants in the Lower Area of Ie Seu-Um Geothermal Outflow, Indonesia. *Malacca Pharmaceutics* 2023;1:55–61. https://doi.org/10.60084/mp.v1i2.44.

[8] Pryshchepa O, Pomastowski P, Buszewski B. Silver Nanoparticles : Synthesis , Investigation Techniques , and Properties. *Advances in Colloid and Interface Science* 2020;284:87–100. https://doi.org/10.1016/j.cis.2020.102246.

[9] Jaswal T, Gupta J. A Review on the Toxicity of Silver Nanoparticles on Human Health. *Materials Today: Proceedings* 2021. https://doi.org/10.1016/j.matpr.2021.04.266.

[10] Salsabila I, Khairan K, Kemala P, Idroes GM, Isnaini N, Maulydia NB, et al. Hybrid Handwash with Silver Nanoparticles from Calotropis Gigantea Leaves and Patchouli Oil: Development and Properties. *Malacca Pharmaceutics* 2024;2:52–62. https://doi.org/10.60084/mp.v2i2.206.

[11] Abubakar A, Yusuf H, Syukri M, Nasution R, Karma T, Munawar AA, et al. Chemometric Classification of Geothermal and Non-Geothermal Ethanol Leaf Extract of Seurapoh (Chromolaena Odorata Linn) Using Infrared Spectroscopy. *IOP Conference Series: Earth and Environmental Science* 2021;667:012070. https://doi.org/10.1088/1755-1315/667/1/012070.

[12] Nuraskin C, Marlina, Idroes R, Soraya C, Djufri. Identification of Secondary Metabolite of Laban Leaf Extract (Vitex Pinnata L) from Geothermal Areas and Non-Geothermal of Agam Mountains in Aceh Besar, Aceh Province, Indonesia. *Rasayan Journal of Chemistry* 2020;13:18–23. https://doi.org/10.31788/RJC.2020.1315434.

[13] Harera CF, Maysarah H, Kemala P, Idroes GM, Maulydia NB, Patwekar M, et al. Geothermal Flora and AgNPs Synergy: A Study on the Efficacy of Lantana Camara and Acrostichum Aureum-Infused Hand Sanitizers. *Grimsa Journal of Science Engineering and Technology* 2024;2:52–9. https://doi.org/10.61975/gjset.v2i2.38.

[14] Idroes GM, Khairan K, Suhartono E, Prasetio R, Idroes GM, Suhendrayatna S. Resilience and Adaptation: Plant Ecology in Indonesia's Geothermal Environments. *Leuser Journal of Environmental Studies* 2025;3:44–55. https://doi.org/10.60084/ljes.v3i1.294.

[15] Kemala P, Idroes R, Khairan K, Ramli M, Ginting B, Helwani Z, et al. Eco-Friendly Synthesis of Silver Nanoparticles: Enhancing Optimization Reaction, Characterization, and Antimicrobial Properties with Lantana Camara from Geothermal Area. *South African Journal of Chemical Engineering* 2025;51:57–67. https://doi.org/10.1016/j.sajce.2024.11.002.

[16] Parmar A, Kapil S, Sachar S, Sharma S. Design of Experiment Based Methodical Optimization and Green Syntheses of Hybrid Patchouli Oil Coated Silver Nanoparticles for Enhanced Antibacterial Activity. *Current Research in Green and Sustainable Chemistry* 2020;3:100016. https://doi.org/10.1016/j.crgsc.2020.100016.

[17] Kemala P, Khairan K, Ramli M, Helwani Z, Rusyana A, Lubis VF, et al. Optimizing Antimicrobial Synergy: Green Synthesis of Silver Nanoparticles from Calotropis Gigantea Leaves Enhanced by Patchouli Patchouli Oil. *Narra J* 2024;4:e800.

[18] Li X, Wang L, Wang B. Optimization of Encapsulation Efficiency and Average Particle Size of Hohenbuehelia Serotina Polysaccharides Nanoemulsions Using Response Surface Methodology. *Food Chemistry* 2017;229:479–86. https://doi.org/https://doi.org/10.1016/j.foodchem.2017.02.051.

[19] Homayoonfal M, Khodaiyan F, Mousavi M. Modelling and Optimising of Physicochemical Features of Walnut-Oil Beverage Emulsions by Implementation of Response Surface Methodology: Effect of Preparation

Conditions on Emulsion Stability. *Food Chemistry* 2015;174:649–59. https://doi.org/https://doi.org/10.1016/j.foodchem.2014.10.117.

[20] Nisah K, Fahrina A, Rizki DR, Puspita K. Optimization of Starch—κ-Carrageenan Hybrid Film as Drug Delivery System Using Response Surface Method. *Heca Journal of Applied Sciences* 2023;1:19–23. https://doi.org/https://doi.org/10.60084/hjas.v1i1.10.

[21] Helwani Z, Amraini SZ, Abd Rahman S, Zahrina I, Julhijah N, Ulfaa SM. Environmental Benefits of Palm Oil Biodiesel Enhancement: Urea Complexation Optimization via RSM. *Leuser Journal of Environmental Studies* 2024;2:62–74. https://doi.org/10.60084/ljes.v2i2.214.

[22] Adameyo, Igbalaye, Awote, Saibu, Kanmodi, Shittu, et al. Antidiabetic, Anti-Inflammatory and Antioxidant Potential of Green Synthesized Silver Nanoparticles Using Fresh Aqueous Leaf Extract of Chromolaena Odorata. *International Journal of Research and Review* 2022;9:182–93. https://doi.org/10.52403/ijrr.20220526.

[23] Musman M. Kimia bahan alam laut. Banda Aceh: Syiah Kuala University Press; 2013.

[24] Indriaty, Djufri, Ginting B, Hasballah K. Phytochemical Screening , Phenolic and Flavonoid Content , and Antioxidant Activity of Rhizophoraceae Methanol Extract from Langsa , Aceh , Indonesia. *Biodiversitas* 2023;24:2865–76. https://doi.org/10.13057/biodiv/d240541.

[25] Sorubavalli U, Vadivazhagi MK, Vadivelu J. Antioxidant and Antimicrobial Activity of Calotrophis Mediated Silver Nanoparticles. *Journal Of Composition Theory* 2019;XII:303–12.

[26] Burlec AF, Hancianu M, Macovei I, Mircea C, Fifere A, Turin-Moleavin I-A, et al. Eco-Friendly Synthesis and Comparative In Vitro Biological Evaluation of Silver Nanoparticles Using Tagetes Erecta Flower Extracts. *Applied Sciences* 2022;12. https://doi.org/https://doi.org/10.3390/app12020887.

[27] Nayem SMA, Sultana N, Haque A, Miah B, Hasan M, Islam T, et al. Green Synthesis of Gold and Silver Nanoparticles by Using Amorphophallus Paeoniifolius Tuber Extract and Evaluation of Their Antibacterial Activity. *Molecules* 2020;25:1–14. https://doi.org/10.3390/molecules25204773.

[28] Mare AD, Man A, Ciurea CN, Toma F, Cighir A, Bert L. Silver Nanoparticles Biosynthesized with Spruce Bark Extract — A Molecular Aggregate with Antifungal Activity against Candida Species 2021:1–14.

[29] Idroes R, Yusuf M, Alatas M, Subhan, Lala A, Muhammad, et al. Geochemistry of Sulphate Spring in the Ie Jue Geothermal Areas at Aceh Besar District, Indonesia. IOP Conference Series: Materials Science and Engineering 2019;523:012012. https://doi.org/10.1088/1757-899X/523/1/012012.

[30] Kemala P, Idroes R, Khairan K, Tallei TE, Ramli M, Efendi R. Green Synthesis of Silver Nanoparticles Using Calotropis gigantea And Its Characterization Using UV-Vis Spectroscopy. IOP Conf. Ser. Earth Environ. Sci., vol. 951, 2021, p. 012090. https://doi.org/10.1088/1755-1315/951/1/012090.

[31] Olawale F, Olofinsan K, Iwaloye O. Biological Activities of Chromolaena Odorata: A Mechanistic Review. *South African Journal of Botany* 2022;144:44–57. https://doi.org/https://doi.org/10.1016/j.sajb.2021.09.001.

[32] Venkatachalam S. Chapter 6. Ultraviolet and visible spectroscopy studies of nanofillers and their polymer nanocomposites. Elsevier Inc.; 2016. https://doi.org/10.1016/B978-0-323-40183-8.00006-9.

[33] Rakib-Uz-Zaman SM, Apu EH, Muntasir MN, Mowna SA, Khanom MG, Jahan SS, et al. Biosynthesis of Silver Nanoparticles from Cymbopogon Citratus Leaf Extract and Evaluation of Their Antimicrobial Properties. *Challeges* 2022;13:http://doi.org/10.3390/challe13010018.

[34] Al-otibi F, Al-ahaidib RA, Alharbi RI, Al-otaibi RM, Albasher G. Antimicrobial Potential of Biosynthesized Silver Nanoparticles by Aaronsohnia Factorovskyi Exract. *Molecules* 2021;26:1–13. https://doi.org/https://doi.org/10.3390/molecules26010130.

[35] Alahmad A, Al-zereini WA, Hijazin TJ, Al-madanat OY, Alghoraibi I, Al-qaralleh O, et al. Green Synthesis of Silver Nanoparticles Using Hypericum Perforatum L . Aqueous Extract with the Evaluation of Its Antibacterial Activity against Clinical and Food Pathogens. *Pharmaceutics* 2022;14. https://doi.org/10.3390/pharmaceutics14051104.

[36] Fertahi S, Ilsouk M, Zeroual Y, Oukarroum A. Recent Trends in Organic Coating Based on Biopolymers and Biomass for Controlled and Slow Release Fertilizers. *Journal of Controlled Release* 2021;330:341–61. https://doi.org/10.1016/j.jconrel.2020.12.026.

[37] Govindan L, Anbazhagan S, Altemimi AB, Lakshminarayanan K, Kuppan S, Pratap-Singh A, et al. Efficacy of Antimicrobial and Larvicidal Activities of Green Synthesized Silver Nanoparticle Using Leaf Extract of Plumbago Auriculata Lam. *Plants* 2020;9. https://doi.org/10.3390/plants9111577.

[38] Kemala P, Khairan K, Ramli M, Idroes GM, Mirda E, Ningsih DS, et al. Characterizing the Size Distribution of Silver Nanoparticles Biofabricated Using Calotropis Gigantea from Geothermal Zone. *Heca Journal of Applied Sciences* 2023;1:30–6. https://doi.org/10.60084/hjas.v1i2.21.

[39] Khairan K, Hasan M, Idroes R, Muhamamd D. Fabrication and Evaluation of Polyvinyl Alcohol / Corn Nanoparticles Biosynthesized in Pogostemon Cablin Benth. *Molecules* 2023;28.

[40] Majeed SA, Sekhosana KE, Tuhl A. Progress on Phthalocyanine-Conjugated Ag and Au Nanoparticles: Synthesis, Characterization, and Photo-Physicochemical Properties. *Arabian Journal of Chemistry* 2020;13:8848–87. https://doi.org/10.1016/j.arabjc.2020.10.014.

[41] Gemishev O, Panayotova M, Gicheva G, Mintcheva N. Green Synthesis of Stable Spherical Monodisperse Silver Nanoparticle Using a Cell-Free Extract of Trichoderma Reesei. *Materials* 2022;15. https://doi.org/https://doi.org/10.3390/mal15020481.

[42] Ali EM, Abdallah BM. Effective Inhibition of Candidiasis Using an Eco- Friendly Leaf Extract of Calotropis-Gigantean-Mediated Silver Nanoparticles. *Nanomaterials* 2020;10:1–16. https://doi.org/10.3390/nano10030422.

[43] Tanase C, Berta L, Coman A, Ros I, Man A, Toma F, et al. Antibacterial and Antioxidant Potential of Silver Nanoparticles Biosynthesized Using the Spruce Bark Extract. *Nanomaterials* 2019;9. https://doi.org/10.3390/nano9111541.

[44] Kemala P, Idroes R, Khairan K, Ramli M, Jalil Z, Idroes GM, et al. Green Synthesis and Antimicrobial Activities of Silver Nanoparticles Using Calotropis Gigantea from Ie Seu-Um Geothermal Area, Aceh Province, Indonesia. *Molecules (Basel, Switzerland)* 2022;27:1–13. https://doi.org/10.3390/molecules27165310.

[45] Kartini K, Alviani A, Anjarwati D, Fanany AF, Sukweenadhi J, Avanti C. Process Optimization for Green Synthesis of Silver Nanoparticles Using Indonesian Medicinal. *Processes* 2020;8. https://doi.org/10.3390/pr8080998.

[46] Alkhathlan AH, Al-abdulkarim HA, Khan M, Khan M. Ecofriendly Synthesis of Silver Nanoparticles Using Aqueous Extracts of Zingiber o Ffi Cinale (Ginger) and Nigella Sativa L . Seeds (Black Cumin) and Comparison of Their Antibacterial Potential. *Sustainability* 2020;12. https://doi.org/10.3390/su122410523.

[47] Haggag EG, Elshamy AM, Rabeh MA, Gabr NM, Salem M, Youssif KA, et al. Antiviral Potential of Green Synthesized Silver Nanoparticles of Lampranthus Coccineus And Malephora Lutea. *International Journal of Nanomedicine* 2019;14:6217–29. https://doi.org/10.2147/IJN.S214171.

[48] Vorobyova V, Vasyliev G, Uschapovskiy D, Lyudmyla K, Skiba M. Green Synthesis, Characterization of Silver Nanoparticals for Biomedical Application and Environmental Remediation. *Journal of Microbiological Methods* 2022;193:106384. https://doi.org/10.1016/j.mimet.2021.106384.

[49] Urnukhsaikhan E, Bold BE, Gunbileg A, Sukhbaatar N, Mishig-Ochir T. Antibacterial Activity and Characteristics of Silver Nanoparticles Biosynthesized from Carduus Crispus. *Scientific Reports* 2021;11:1–12. https://doi.org/10.1038/s41598-021-00520-2.

[50] Salleh A, Naomi R, Utami ND, Mohammad AW, Mahmoudi E, Mustafa N, et al. The Potential of Silver Nanoparticles for Antiviral and Antibacterial Applications: A Mechanism of Action. *Nanomaterials* 2020;10:1–20. https://doi.org/10.3390/nano10081566.

[51] Ajlouni A-W, Hamdan EH, Eid ARA, Shaik MR, Khan M, Kuniyil M, et al. Green Synthesis of Silver Nanoparticles Using Aerial Part Extract of the Anthemis Pseudocotula Boiss. Plant and Their Biological Activity. *Molecules* 2023;28. https://doi.org/https://doi.org/10.3390/molecules28010246.

[52] Gaddam S, Kotakadi VS, D.V.R. S, Yakkate S, Reddy A. Efficient and Robust Biofabrication of Silver Nanoparticles by Cassia Alata Leaf Extract and Their Antimicrobial Activity. *Journal of Nanostructure Chemistry* 2014;4:1–9. https://doi.org/10.1007/s40097-014-0082-5.

[53] Rodriguez-Loya J, Lerma M, Gardea-Torresdey JL. Dynamic Light Scattering and Its Application to Control Nanoparticle Aggregation in Colloidal Systems: A Review. *Micromachines* 2024;15. https://doi.org/10.3390/mi15010024.

[54] Filippov SK, Khusnutdinov R, Murmiliuk A, Inam W, Zakharova LY, Zhang H, et al. Dynamic Light Scattering and Transmission Electron Microscopy in Drug Delivery: A Roadmap for Correct Characterization of Nanoparticles and Interpretation of Results. *Materials Horizons* 2023;10:5354–70. https://doi.org/10.1039/d3mh00717k.

[55] Teulon JM, Godon C, Chantalat L, Moriscot C, Cambedouzou J, Odorico M, et al. On the Operational Aspects of Measuring Nanoparticle Sizes. *Nanomaterials* 2019;9. https://doi.org/10.3390/nano9010018.

[56] He L, Zahn DRT, Madeira TI. Photocatalytic Performance of Sol-Gel Prepared TiO2 Thin Films Annealed at Various Temperatures. *Materials* 2023;16. https://doi.org/10.3390/ma16155494.

[57] Bishoyi AK, Sahoo CR, Samal P, Mishra NP, Jali BR, Khan MS, et al. Unveiling the Antibacterial and Antifungal Potential of Biosynthesized Silver Nanoparticles from Chromolaena Odorata Leaves. *Scientific Reports* 2024;14:1–15. https://doi.org/10.1038/s41598-024-57972-5.

[58] Tripathi N, Goshisht MK. Recent Advances and Mechanistic Insights into Antibacterial Activity, Antibiofilm Activity, and Cytotoxicity of Silver Nanoparticles. *ACS Applied Bio Materials* 2022;5:1391–463. https://doi.org/10.1021/acsabm.2c00014.

[59] Kantarciyan A, Segovia-Campos I, Slaveykova VI. Evaluating Cell Surface Extraction Methods for Improved Assessment of Silver Nanoparticle Bioaccumulation. *Aquatic Toxicology* 2025;283:107340. https://doi.org/https://doi.org/10.1016/j.aquatox.2025.107340.

[60] Ding S, Zheng L, Tao T, Li Q, Cai J, Zhou Q, et al. Silver Nanoparticles Priming for Drought Tolerance in Wheat: Insights from Antioxidant System Activation and Stress Memory. *Chemical and Biological Technologies in Agriculture* 2025;12:57. https://doi.org/10.1186/s40538-025-00778-y.

[61] Jaffar SS, Saallah S, Misson M, Siddiquee S, Roslan J, Lenggoro W. Green Synthesis of Flower-Like Carrageenan-Silver Nanoparticles and Elucidation of Its Physicochemical and Antibacterial Properties. *Molecules* 2023;28. https://doi.org/10.3390/molecules28020907.